Ypt1/Rab1 regulates Hrr25/CK1δ kinase activity in ER–Golgi traffic and macroautophagy

Juan Wang,[1] Saralin Davis,[1] Shekar Menon,[1] Jinzhong Zhang,[1] Jingzhen Ding,[1] Serena Cervantes,[1] Elizabeth Miller,[2] Yu Jiang,[3] and Susan Ferro-Novick[1]

[1]Department of Cellular and Molecular Medicine, Howard Hughes Medical Institute, University of California, San Diego, La Jolla, CA 92093
[2]Department of Biological Sciences, Columbia University, New York, NY 10027
[3]Department of Pharmacology and Chemical Biology, University of Pittsburgh School of Medicine, Pittsburgh, PA 15261

ER-derived COPII-coated vesicles are conventionally targeted to the Golgi. However, during cell stress these vesicles also become a membrane source for autophagosomes, distinct organelles that target cellular components for degradation. How the itinerary of COPII vesicles is coordinated on these pathways remains unknown. Phosphorylation of the COPII coat by casein kinase 1 (CK1), Hrr25, contributes to the directional delivery of ER-derived vesicles to the Golgi. CK1 family members are thought to be constitutively active kinases that are regulated through their subcellular localization. Instead, we show here that the Rab GTPase Ypt1/Rab1 binds and activates Hrr25/CK1δ to spatially regulate its kinase activity. Consistent with a role for COPII vesicles and Hrr25 in membrane traffic and autophagosome biogenesis, *hrr25* mutants were defective in ER–Golgi traffic and macroautophagy. These studies are likely to serve as a paradigm for how CK1 kinases act in membrane traffic.

Introduction

The fidelity of vesicle traffic relies on the coordinated action of multiple trafficking machinery components. Vesicle budding is initiated when cytosolic coat proteins assemble on a membrane to capture cargo into a vesicle and facilitate vesicle budding (Zanetti et al., 2012). Our recent studies have revealed that coat proteins and protein phosphorylation play a key role in ordering vesicle targeting and fusion events (Lord et al., 2011; Bhandari et al., 2013). Focusing on the role of the COPII coat complex in directing ER-derived vesicles to the Golgi complex, we have shown that phosphorylation of the COPII coat by the casein kinase 1 (CK1) family member Hrr25 contributes to the directional delivery of ER-derived vesicles to the Golgi (Lord et al., 2011). CK1 kinases represent a unique group of serine/threonine protein kinases whose regulation and role in membrane traffic are largely unknown (Knippschild et al., 2005).

COPII vesicles form upon hierarchical assembly of the COPII coat: GTP-activated Sar1 (Sar1-GTP) recruits the cargo adaptor complex, Sec23/Sec24, which in turn recruits the outer coat complex, Sec13/Sec31 (Zanetti et al., 2012). After vesicle scission, COPII-coated vesicles conventionally fuse with the Golgi. However, a growing body of evidence indicates that, during cell stress, some of these vesicles are diverted to the macroautophagy pathway where they fuse with another compartment, most likely Atg9 vesicles, to initiate phagophore formation (Graef et al., 2013; Tan et al., 2013; Ge et al., 2014). In the canonical pathway for COPII vesicles, the direction of ER–Golgi traffic is controlled by sequential interactions of the Sec23 subunit with three different regulators: Sar1-GTP; TRAPPI, the multimeric guanine nucleotide exchange factor (GEF) for the GTPase Ypt1; and Hrr25, a serine-threonine kinase that regulates ER–Golgi traffic (Murakami et al., 1999; Lord et al., 2011). All three partners compete with each other for interaction with Sec23 by a conserved mechanism (Lord et al., 2011). TRAPPI-mediated activation of Ypt1 (Rab1 in mammals) on the vesicle leads to the recruitment of an effector, Uso1 (p115 in mammals), which physically links the vesicle to the Golgi (Ballew et al., 2005). Prior to fusion, multiple coat subunits are phosphorylated by Hrr25, a CK1 kinase that localizes to the Golgi at steady state and is thought to be constitutively active (Lord et al., 2011; Bhandari et al., 2013).

Here, we show that Ypt1 directly recruits Hrr25 to COPII vesicles to activate it on two different pathways, ER to Golgi and the catabolic pathway called macroautophagy that is induced in response to cell stress (Nakatogawa et al., 2009). By temporally and spatially regulating Hrr25 kinase activity, Ypt1 ensures that only the vesicle-borne pool of the coat is phosphorylated. Thus the kinase activity of Hrr25, which was previously thought to be constitutively active (Knippschild et al., 2005), is instead regulated by a member of the Rab GTPase family. Our

Correspondence to Susan Ferro-Novick: sfnovick@ucsd.edu

S. Menon's present address is Affymetrix, Inc., Santa Clara, CA 95051.

Abbreviations used in this paper: Ape1, aminopeptidase I; CIP, calf intestinal phosphatase; CK1, casein kinase 1; GEF, guanine nucleotide exchange factor; PAS, preautophagosomal structure.

The Rockefeller University Press $30.00
J. Cell Biol. Vol. 210 No. 2 273–285
www.jcb.org/cgi/doi/10.1083/jcb.201408075

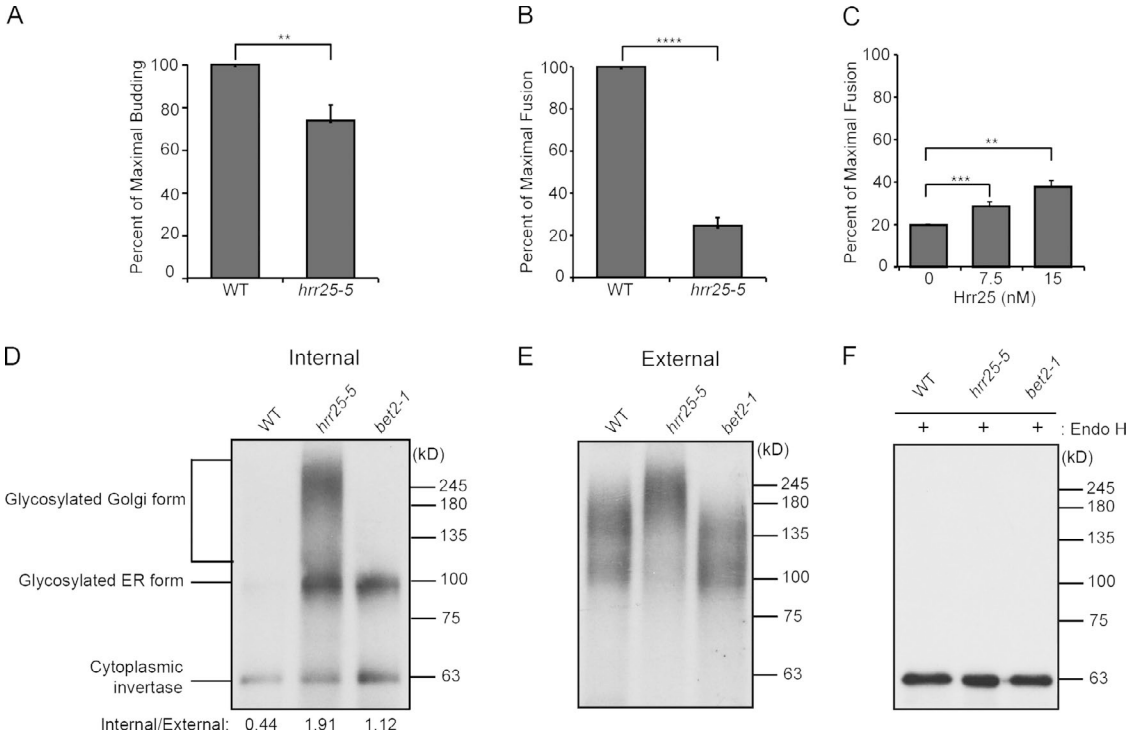

Figure 1. **Hrr25 is required for ER–Golgi traffic in vivo and COPII vesicle fusion in vitro**. (A) Vesicle budding and (B) fusion were measured in vitro in WT (SFNY2051) and *hrr25-5* mutant (SFNY 2049) fractions as described in the Materials and methods. (C) Increasing concentrations of purified recombinant His_6-Hrr25 were incubated with a mutant S1 fraction for 30 min on ice before the transport assay was performed. (A–C) Error bars represent SD; $n = 3$; **, $P < 0.01$; ***, $P < 0.001$; ****, $P < 0.0001$, Student's *t* test. Internal (D) and external (E) forms of invertase were examined in WT (SFNY 2330), *hrr25-5* (SFNY 2329), and *bet2-1* (SFNY 92) mutant cells. The ratio of internal to external invertase is reported at the bottom of each lane. (F) The external form of invertase secreted in WT, *hrr25-5*, and *bet2-1* mutant cells was treated with endoglycosidase H (Endo H).

findings raise the intriguing possibility that the activity of other members of this kinase family, that regulate membrane traffic, may also be modulated by Rab GTPases.

Results

The *hrr25-5* mutant is defective in COPII vesicle fusion

We previously showed that the ATP competitive inhibitor, IC261, disrupts ER–Golgi vesicle fusion in vitro (Lord et al., 2011). Although IC261 selectively inhibits the highly conserved kinase domain of CKIδ, it also inhibits the function of other kinases, albeit significantly less effectively (Mashhoon et al., 2000). Therefore, to more directly probe the role of Hrr25 in ER–Golgi traffic, we analyzed vesicle budding and fusion in vitro using fractions isolated from the *hrr25-5* mutant, which we recently showed impairs Hrr25 kinase activity in vivo (Bhandari et al., 2013) and in vitro (Fig. S1 A).

Fractions prepared from mutant cells displayed a small but significant decrease in COPII budding efficiency (Fig. 1 A) and a dramatic defect in vesicle fusion with the Golgi (Fig. 1 B). The defect in fusion is consistent with earlier studies implicating Hrr25 in COPII vesicle uncoating (Lord et al., 2011). The diminished fusion activity was partially restored by the addition of purified recombinant Hrr25 (Fig. 1 C). The defect in vesicle formation was somewhat surprising because our previous studies with IC261 showed it stimulated vesicle budding in vitro (Lord et al., 2011). These differential effects could derive from experimental differences associated with using an inhibitor that rapidly blocks kinase activity versus a mutant where coat proteins are most likely constitutively hypophosphorylated. Indeed, when we probed lysates prepared from the *hrr25-5* mutant for COPII coat subunits (Fig. S1 B), several subunits (Sec31, Lst1, and Sec23) were reduced in abundance relative to WT or were partially degraded (Sec24). Although the hypophosphorylated coat complex appeared to be less stable, it was still efficiently recruited to ER exit sites in the *hrr25-5* mutant (Fig. S1 C).

To assess the consequence of disrupting Hrr25 function in vivo, we monitored the trafficking of invertase. There are two forms of invertase, a cytoplasmic and secreted form. The secreted form is induced in low-glucose medium, and then traffics from the ER to the Golgi before it is released into the periplasm (Novick and Schekman, 1979). When we analyzed invertase trafficking in the *hrr25-5* mutant in vivo, we saw delays in both ER–Golgi and Golgi traffic (Fig. 1 D). Accumulation of the ER form of invertase in the *hrr25-5* mutant was comparable to that of *bet2-1*, a secretory mutant that is defective in the prenylation of Ypt1 (Rossi et al., 1991). Failure to prenylate Ypt1 leads to a loss of Ypt1 function (Rossi et al., 1991). The *hrr25-5* mutant also accumulated an intracellular Golgi form of invertase that migrated slower on an SDS polyacrylamide gel than the form observed in WT. Treatment of this form of invertase with the enzyme endoglycosidase H, which removes N-linked carbohydrate (Trimble and Maley, 1977), confirmed that invertase in the *hrr25-5* mutant is hyperglycosylated (compare Fig. 1, E and F). Together these findings imply that Hrr25 is required for the proper trafficking of secretory proteins from the ER to the Golgi complex and through the Golgi complex. Our in vitro studies

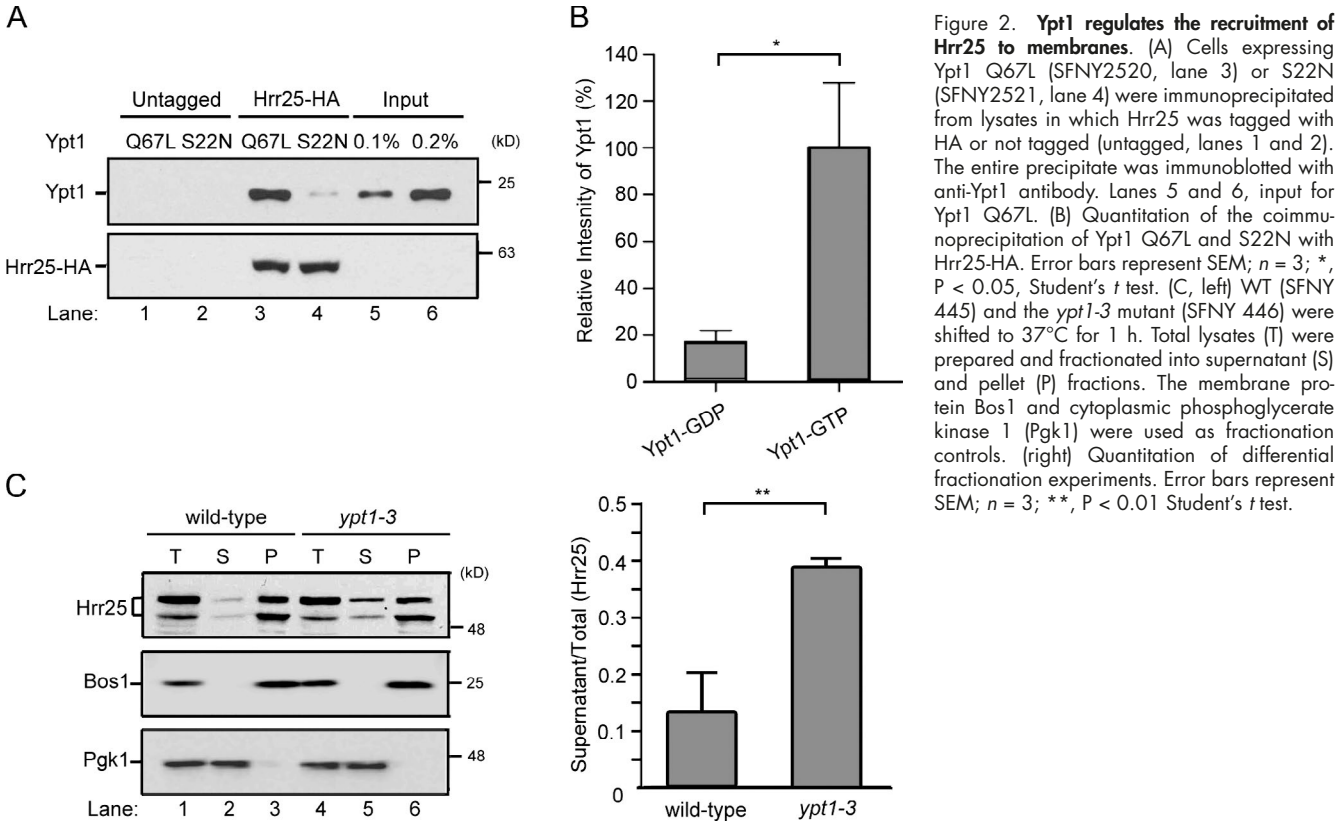

Figure 2. **Ypt1 regulates the recruitment of Hrr25 to membranes**. (A) Cells expressing Ypt1 Q67L (SFNY2520, lane 3) or S22N (SFNY2521, lane 4) were immunoprecipitated from lysates in which Hrr25 was tagged with HA or not tagged (untagged, lanes 1 and 2). The entire precipitate was immunoblotted with anti-Ypt1 antibody. Lanes 5 and 6, input for Ypt1 Q67L. (B) Quantitation of the coimmunoprecipitation of Ypt1 Q67L and S22N with Hrr25-HA. Error bars represent SEM; $n = 3$; *, $P < 0.05$, Student's t test. (C, left) WT (SFNY 445) and the *ypt1-3* mutant (SFNY 446) were shifted to 37°C for 1 h. Total lysates (T) were prepared and fractionated into supernatant (S) and pellet (P) fractions. The membrane protein Bos1 and cytoplasmic phosphoglycerate kinase 1 (Pgk1) were used as fractionation controls. (right) Quantitation of differential fractionation experiments. Error bars represent SEM; $n = 3$; **, $P < 0.01$ Student's t test.

indicate that the defect in ER–Golgi traffic is a consequence of a block in COPII vesicle fusion.

The recruitment of Hrr25/CK1δ to membranes is regulated by Ypt1/Rab1

Previous studies suggested that the COPII coat is phosphorylated as it comes into proximity with Golgi-localized Hrr25 (Lord et al., 2011). However, the recent observation that COPII vesicles can contribute to more than one membrane trafficking pathway (Graef et al., 2013; Tan et al., 2013; Ge et al., 2014) prompted us to test if Hrr25 is directly recruited to COPII vesicles. Because Ypt1/Rab1 is a key driver of effector recruitment to vesicles, we first tested whether Hrr25 can interact with Ypt1 by introducing GTP (Q67L)- and GDP (S22N)-locked forms of Ypt1 into cells expressing Hrr25-HA. Hrr25-HA preferentially coprecipitated the GTP-locked form of Ypt1 (Fig. 2, A and B), implying that Hrr25 is an effector of Ypt1.

To begin to address the effect of Ypt1 on Hrr25 in vivo, we examined the intracellular distribution of Hrr25 in the temperature-sensitive (ts) *ypt1-3* mutant. WT and mutant cells were incubated for 1 h at 37°C and lysates were fractionated by differential centrifugation into high-speed soluble and insoluble fractions. We observed a significant and reproducible increase in the soluble pool of Hrr25 in *ypt1-3* mutant cells that were shifted to 37°C (Fig. 2 C; also see fluorescence in Fig. 5 A), whereas no significant increase was observed in permissively grown (23°C) cells (Fig. S1 D).

The role of Hrr25 in membrane traffic appears to be highly conserved (Lord et al., 2011). To address if the interaction between Hrr25 and Ypt1 is conserved in mammalian cells, we incubated purified recombinant GST-CK1δ with the GTP- and GDP-locked forms of Rab1a (Fig. 3 A and Fig. S1 E) and found that GST-CK1δ only bound to Rab1a Q70L (compare lanes 2–5 with lanes 10–13). Although Rab1a Q70L bound to GST-CK1δ, it did not bind to GST (lanes 6 and 7). Additionally, although GST-CK1δ bound specifically to Rab1a, it did not bind to Rab2a or Rab4a (Fig. 3 B and Fig. S1 F).

To address if Rab1 also plays a role in recruiting CK1δ to membranes, we used shRNA to deplete HeLa cells of Rab1a, and then examined the intracellular distribution of CK1δ. Cells were depleted of Rab1a using an shRNA construct (Fig. 3 C) that was previously shown to target and knock down Rab1a (Ishida et al., 2012). Lysates were prepared from mock and depleted cells and differential fractionation was performed. This analysis revealed that although CK1δ fractionated with membranes in the mock treated cells, a significant fraction of CK1δ was found in the supernatant of the depleted cells (Fig. 3, D and E). The increase in the soluble pool of CK1δ was specifically caused by the loss of Rab1a, as no defect was observed when the fractionation experiment was performed with a lysate prepared from cells treated with an shRNA-resistant construct (Fig. S2, A and B). Similar results were also obtained when we performed these same experiments using two different shRNA constructs that specifically target a subunit of the TRAPP complex, the GEF that activates Rab1 (Fig. S2, C and D). Together, these findings support the hypothesis that Ypt1/Rab1 recruits Hrr25/CK1δ to membranes.

Ypt1 regulates Hrr25 kinase activity on vesicles

Next, we tested if Ypt1 regulates Hrr25 kinase activity. Hrr25-HA was immunoprecipitated from WT and *ypt1-3* mutant cells, and kinase activity was quantitatively measured in vitro using myelin basic protein as a substrate. Although equal amounts of Hrr25-HA were precipitated with anti-HA antibody from both strains (Fig. 4 A), kinase activity was ∼50% of that

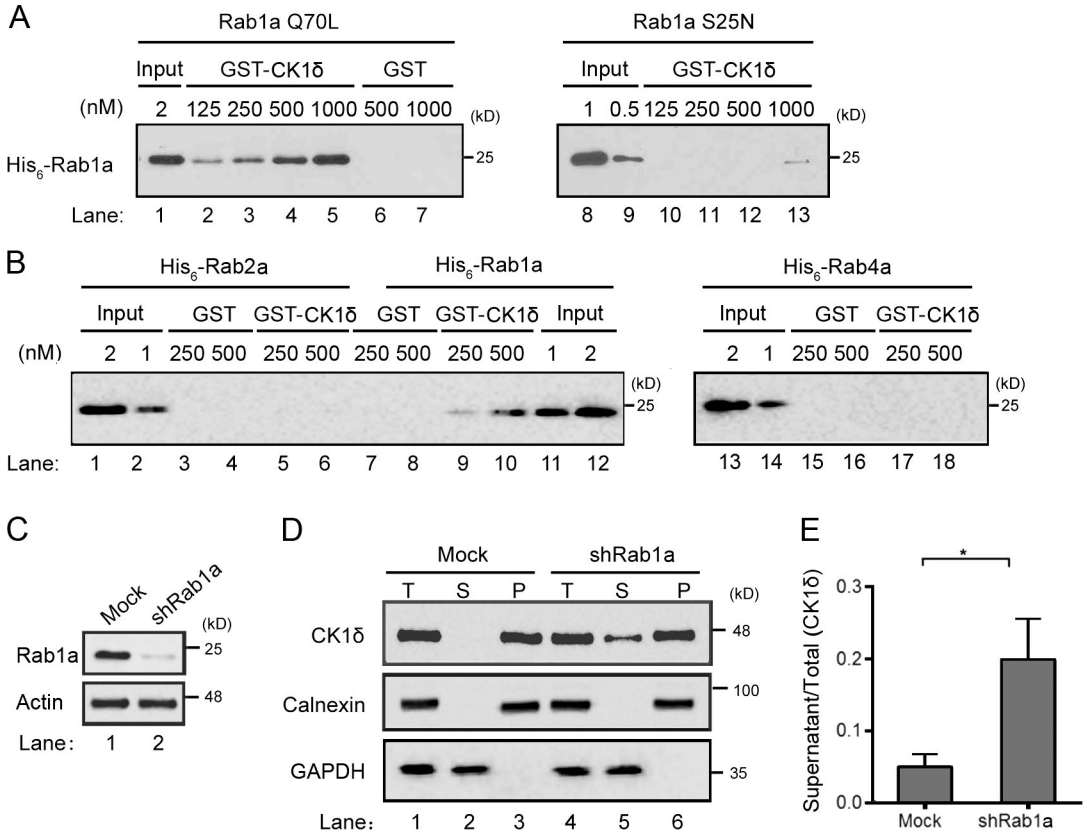

Figure 3. **CK1δ is a Rab1 effector.** (A) Purified GST or GST-CK1δ was incubated with increasing amounts of purified His_6-Rab1a Q70L (left) or His_6-Rab1a S25N (right). (B) Same as A, except His_6-Rab2a, His_6-Rab1a, and His_6-Rab4a were incubated with GST and GST-CK1δ (C) HeLa cells were harvested 96 h after they were mock transfected or transfected with the shRab1a construct. Samples were immunoblotted with anti-Rab1 and anti-actin antibodies. Actin was used as a loading control. In three separate experiments, ~90.1 ± 0.4% of the Rab1a was depleted in the shRNA-treated cells. (D) Lysates (T) were prepared from mock and depleted cells and fractionated as previously described (Bhandari et al., 2013) to produce supernatant (S) and pellet (P) fractions. Western blot analysis was performed to detect CK1δ, calnexin, and the cytoplasmic protein GAPDH in each fraction. (E) Quantitation of differential fractionation. Error bars represent SEM; $n = 4$; *, $P < 0.05$, Student's *t* test.

of WT from permissively grown *ypt1-3* cells and almost completely abrogated after shifting cells to 37°C before Hrr25-HA isolation (Fig. 4 B). Control experiments revealed that kinase activity was dependent on the presence of the HA tag (Fig. 4 A, compare lane 1 and 2). Additionally, we could not detect activity above background levels with kinase deficient Hrr25 (Hrr25-5-HA) cells (Fig. S3 A). The defect observed in the *ypt1-3* mutant appeared to be specific for Ypt1 and not other Rabs, as no defect in kinase activity was observed when Hrr25-HA was precipitated from the *sec4-8* and *ypt32Δypt31*^{ts} mutants (Fig. S3 B).

To address if Ypt1 directly activates the kinase activity of Hrr25, we precipitated Hrr25-HA from *ypt1-3* cells grown at 23°C or shifted to 37°C and then incubated the kinase with non-prenylated activated Ypt1-His_6 (Q67L). Interestingly, activated Ypt1 (Fig. 4 C), but not WT Ypt1, which is largely in the inactive or GDP-bound form (Fig. 4 D), completely restored activity when the kinase was precipitated from permissively grown *ypt1-3* cells. Activated Ypt1 also restored activity, albeit less efficiently, when Hrr25-HA was precipitated from *ypt1-3* cells that were incubated at 37°C for 2 h (Fig. S3 C). Together these findings imply that Ypt1 may directly regulate the kinase activity of Hrr25.

If Ypt1 regulates Hrr25 kinase activity and its recruitment to membranes, the COPII coat should be hypophosphorylated when Ypt1 is inactivated in the *ypt1-3* mutant. To test this possibility, we examined the mobility of the most readily detected Hrr25 substrate, the Sec24 homologue Lst1 (Shimoni et al., 2000; Bhandari et al., 2013), whose phosphorylation can be monitored by a gel shift as previously described (Bhandari et al., 2013). Lst1 isolated from the *ypt1-3* mutant after a 1-h shift to 37°C migrated faster than the WT control (Fig. 4 E, compare lanes 1 and 2). This increase in mobility was a result of decreased phosphorylation, as Lst1 from mutant and WT cells had the same mobility after treatment with calf intestinal phosphatase (CIP; Fig. 4 E, lanes 5 and 6), an effect that was abolished when CIP activity was inhibited with EDTA (Fig. 4 E, lanes 7 and 8). We also noted that the distinct lysis conditions used for these immunoprecipitations permitted detection of a stable pool of hypophosphorylated Lst1 in the *ypt1-3* mutant. This contrasts with the conditions used to generate cellular fractions for the in vitro transport assay, where Lst1 and other coat proteins were unstable in this mutant (Fig. S1 B and Fig. S3 D). The effects we observed in immunoprecipitations were specific for Ypt1 as the loss of function of two other Rabs, Sec4 and the redundant Rabs Ypt31/Yp32, did not alter the mobility of Lst1 (Fig. S3 E).

To demonstrate that phosphorylation of the COPII coat occurs on vesicles, the mobility of Lst1 was examined after budding was blocked in the *sec12-4* ts mutant. Lst1 that was precipitated from the mutant after a 1-h shift to 37°C showed a marked decrease in phosphorylation (Fig. 4 E, lanes 3–4 and 9–12). Together, these findings indicate that Ypt1 regulates Hrr25 kinase activity on vesicles to ensure that only the vesicle-bound pool of the coat is phosphorylated.

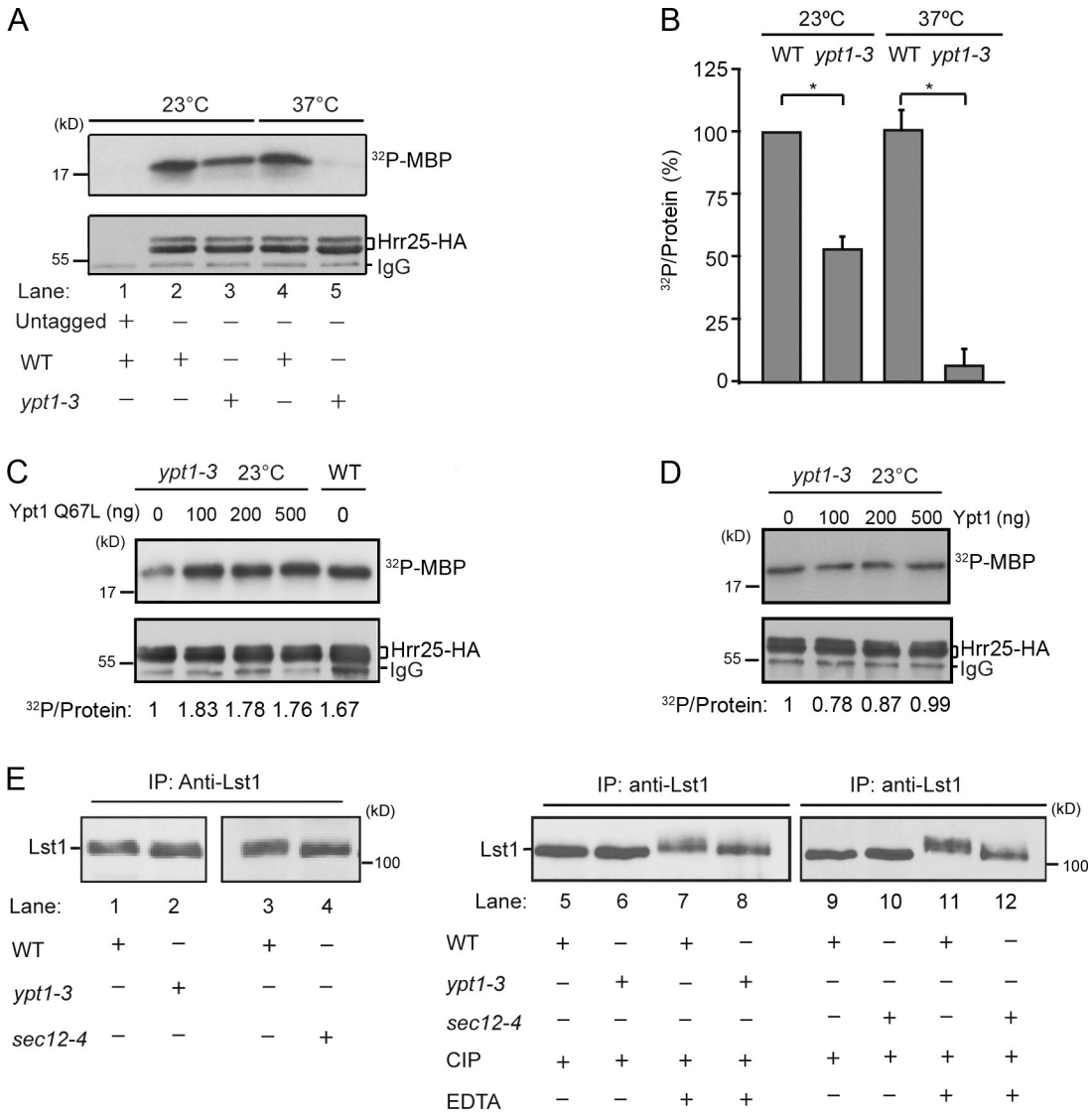

Figure 4. **Ypt1 regulates Hrr25 kinase activity on vesicles**. (A) Hrr25 kinase activity is ts in the *ypt1-3* mutant. WT (SFNY 2443) and mutant (SFNY 2445) cells were grown at 23°C or shifted to 37°C for 2 h. Hrr25-HA was precipitated from lysates onto Protein A–conjugated agarose beads and kinase activity was assayed using MBP as a substrate as described in the Materials and methods. (B) Quantitation of kinase activity from WT and the *ypt1-3* mutant from three separate experiments. The data were normalized to the amount of Hrr25-HA in the precipitate. Error bars represent SD; $n = 3$; *, $P < 0.05$, Student's *t* test. (C and D) Hrr25-HA was precipitated from permissively grown *ypt1-3* cells and preincubated with increasing concentrations of Ypt1 Q67L (C) or Ypt1 (D) for 15 min at 25°C and then assayed as described in the Materials and methods. The ratio of phosphorylated MBP to Hrr25-HA is calculated at the bottom of each lane. Note that the kinase activity of the mutant at 0 ng was set at 1.0. The assays in C and D were performed multiple times. The data that are shown are representative. (E) Lst1 is hypophosphorylated in the *ypt1-3* and *sec12-4* (NY738) mutants. WT and mutant cells were shifted to 37°C for 1 h, lysates were prepared and Lst1 was immunoprecipitated (lanes 1–12). Samples in lanes 5, 6, 9, and 10 were treated with CIP, while samples in lanes 7, 8, 11, and 12 were treated with CIP plus EDTA.

Ypt1 recruits Hrr25 to the macroautophagy pathway

Given recent findings that link COPII-coated membranes to macroautophagy, we asked if Ypt1 might recruit Hrr25 to this pathway. Macroautophagy or nonselective autophagy begins with the de novo formation of a cup-shaped membrane, called the isolation membrane or phagophore, which engulfs intracellular proteins targeted for degradation. These membranes expand and seal to form an autophagosome, a double-membrane structure (Nakatogawa et al., 2009). In the yeast *Saccharomyces cerevisiae*, autophagosomes are formed at a preautophagosomal structure (PAS), an assembly site for *ATG* (autophagy-related) gene products. Most Atg proteins function in both macroautophagy and the selective autophagy pathway called Cvt (cytoplasm to vacuole targeting). These pathways are regulated by the Rab GTPase Ypt1 (Lynch-Day et al., 2010; Barrowman et al., 2010).

In both yeast and mammalian cells, phagophore assembly occurs adjacent to ER exit sites (ERES), a subdomain of the ER where COPII vesicles are produced (Ge et al., 2013; Graef et al., 2013; Suzuki et al., 2013). A growing body of evidence indicates that, during cell stress, some COPII vesicles are diverted to the macroautophagy pathway where they fuse with another compartment, most likely Atg9 vesicles, to initiate phagophore formation (Graef et al., 2013; Tan et al., 2013).

The findings described above imply that Hrr25 functions directly on COPII vesicles and that the steady-state Golgi local-

ization of Hrr25/CK1δ arises from the rapid fusion of COPII vesicles with the Golgi. Because Hrr25 is a Ypt1 effector and COPII vesicles have been implicated in phagophore formation (Tan et al., 2013), we asked if Ypt1 could similarly regulate coat phosphorylation on the macroautophagy pathway. Ypt1 is recruited to the PAS by the autophagy-specific GEF, TRAPPIII (Lynch-Day et al., 2010). TRAPPIII shares six subunits with TRAPPI, plus the unique subunit Trs85, that directs it to the PAS (Lynch-Day et al., 2010; Wang et al., 2013). Like TRAPPI, TRAPPIII binds to the COPII coat subunit Sec23 (Tan et al., 2013). To examine the role of Hrr25 in macroautophagy, we first determined if Hrr25 localizes to the PAS in a Ypt1-dependent manner. When macroautophagy was induced by nitrogen starvation, Hrr25 colocalized with the PAS markers Ape1 (Fig. 5 A and Fig. S4 A, left) and Atg17 in a significant fraction of cells (Fig. S4 A, right). Like other proteins required for autophagy, Hrr25 accumulated at the PAS when the initiation of macroautophagy was blocked in *atg1Δ* and *atg13Δ* mutants (Fig. 5, A and B; and Fig. S4 B). Consistent with the observation that Ypt1/Rab1 regulates the recruitment of Hrr25 to membranes, less Hrr25-GFP was observed at the PAS in *ypt1-2*, a mutant allele of *ypt1* that disrupts macroautophagy but not ER–Golgi traffic (Bacon et al., 1989; Lynch-Day et al., 2010). Hrr25-GFP also appeared to be more cytosolic in this mutant (Fig. 5, A and B). The recruitment of Hrr25-GFP to the PAS was reduced in *atg17Δ* and *trs85Δ* mutants, but not in an *atg9Δ* mutant (Fig. 5, A and B; and Fig. S4 B). This result is consistent with our previous finding that Atg17 recruits TRAPPIII to the PAS via the Trs85 subunit (Wang et al., 2013).

When we blocked vesicle budding from the ER in the *sec12-4* mutant, the recruitment of Hrr25-GFP to the PAS was disrupted to the same extent as in the *ypt1-2* mutant (Fig. 5, A and B). Similar results were obtained when we examined the recruitment of Hrr25 to the PAS in *ypt1* and *sec12* mutants that lack Atg19, the Cvt cargo receptor (*ypt1-2 atg19Δ*, *sec12-4 atg19Δ*; Fig. S4 C). Thus, Hrr25 is still recruited to the PAS by Ypt1 under starvation conditions in the absence of the Cvt pathway.

Using an auxin-inducible degron strain that conditionally knocked-out Hrr25, it was previously reported that Hrr25 is not required for macroautophagy (Tanaka et al., 2014). As the findings described above are not consistent with this earlier report, we used a different *hrr25* mutant (*hrr25-5*) to ask this question. To assess activity, we used the activation of vacuolar alkaline phosphatase activity as a marker to quantitatively measure autophagic activity in the *hrr25-5* mutant. Interestingly, *hrr25-5* displayed a defect in autophagy that was similar to that observed in the *ypt1-2* and *ypt1-3* mutants (Fig. 6 A). Ypt1 and its mammalian homologue Rab1 were previously reported to be required for macroautophagy (Lynch-Day et al., 2010; Winslow et al., 2010). As a second marker for macroautophagy, we analyzed the translocation of GFP-Atg8 to the vacuole. GFP-Atg8 is normally localized in the cytosol and PAS (Kirisako et al., 1999; Suzuki et al., 2001). When macroautophagy is induced, however, GFP-Atg8 is delivered to the vacuole, where it is cleaved, releasing free GFP in the lumen of the vacuole. 2 h after nitrogen starvation, the delivery of GFP-Atg8 to the vacuole was markedly delayed in the *hrr25-5* mutant, and the observed defect was comparable to the *ypt1-2* and *ypt1-3* mutants (Fig. 6 B). Interestingly, in a subset of *hrr25-5* mutant cells, we also saw numerous punctate GFP-Atg8 structures that did not contain Ape1-RFP (Figs. 6 B and 7 C). Superresolution structured illumination microscopy (SIM) revealed that these

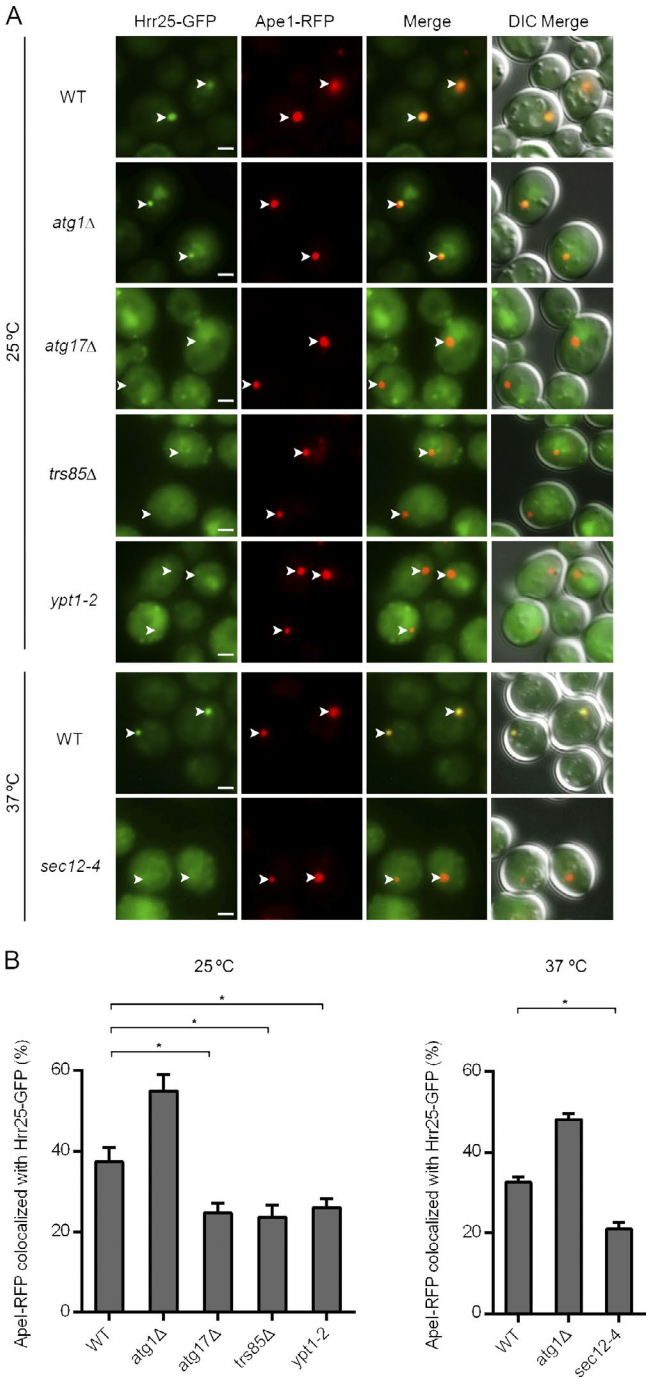

Figure 5. **Ypt1 recruits Hrr25 to the macroautophagy pathway.** (A) Hrr25-GFP appears to be more cytosolic in the *ypt1-2* (SFNY2528) and *sec12-4* (SFNY2569) mutants than WT. For the *ypt1-2* mutant, the WT strain was SFNY2527. For the *sec12-4* mutant, the WT strain was SFNY 2568. Cells expressing Hrr25-GFP and Ape1–RFP were grown to log phase in SC–Leu medium at 25°C and shifted to SD–N medium for 4 h at 25°C. The *sec12-4* mutant and the corresponding WT were shifted to SD–N medium for 2 h at 37°C. Arrowheads point to the PAS, which is marked with Ape1-RFP. Bar, 2 µm. (B) The Apel-RFP that colocalized with Hrr25-GFP was calculated in 450 cells. Error bars represent SEM; $n = 3$; *, $P < 0.05$; Student's *t* test.

punctate structures are not autophagosomes. Additionally, no accumulation of cup-shaped membranes were observed in the *hrr25-5* mutant (Fig. S4 D). We conclude that a defect in macroautophagy was not observed in the auxin-inducible degron

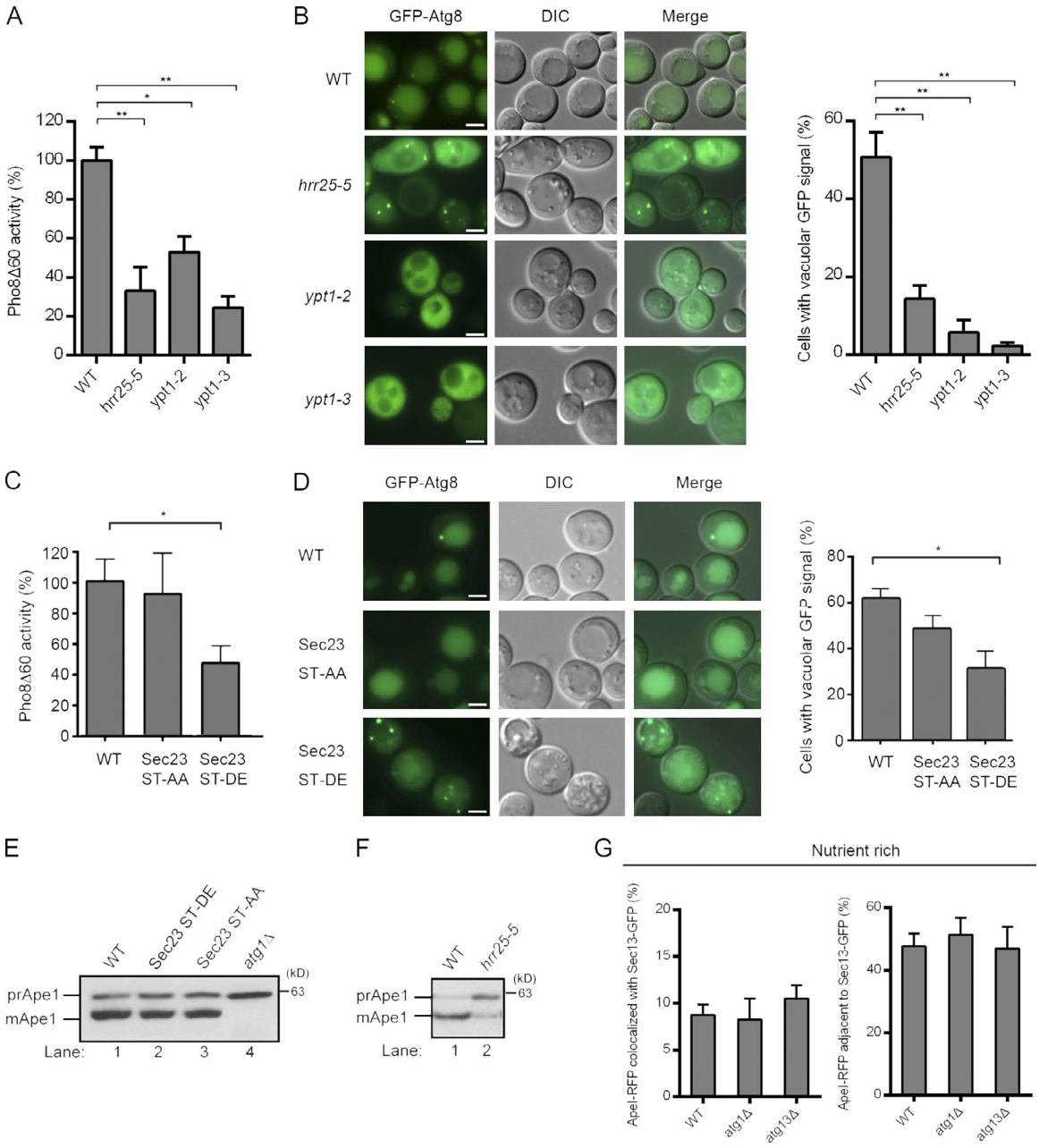

Figure 6. **The COPII coat is required for macroautophagy, but not the Cvt pathway**. (A) Vacuolar alkaline phosphatase activity was assayed in SFNY2529, SFNY2530, SFNY2565, and SFNY2567 as described in the Materials and methods. The activity of WT after 2 h of starvation at 37°C was set as 100% and the activity at time 0 was subtracted. Error bars represent SEM; $n = 3$; *, $P < 0.05$; **, $P < 0.01$, Student's *t* test. (B, left) The translocation of GFP-Atg8 was examined in WT (SFNY 2623), *hrr25-5* (SFNY 2622), *ypt1-2* (SFNY 2660), and *ypt1-3* (SFNY 2662) mutants 2 h after nitrogen starvation at 37°C. Bar, 2 µm. (right) Error bars represent SEM; $n = 3$; **, $P < 0.01$, Student's *t* test. (C) Vacuolar alkaline phosphatase was measured in protein extracts of WT (SFNY2554), the *sec23* phosphomimetic (SFNY 2556), and alanine (SFNY 2555) mutants. Error bars represent SEM; $n = 3$; *, $P < 0.05$ Student's *t* test. (D) The translocation of GFP-Atg8 was examined in WT (SFNY2624) and the *sec23* mutants (SFNY2625, SFNY2626) 1 h after nitrogen starvation at 37°C. Error bars represent SEM; $n = 3$; *, $P < 0.05$, Student's *t* test. Bar, 2 µm. (E and F) Hrr25, but not Sec23, is required on the Cvt pathway (SFNY1950, SFNY1951, SFNY1952, and SFNY2488). Ape1 processing was measured as described in the Materials and methods. (G) WT, *atg1*Δ, and *atg13*Δ cells expressing Sec13-GFP and Ape1-RFP (SFNY2627, SFNY2628, and SFNY2629) were grown to log phase in SC–Leu medium at 25°C. Cells from three separate experiments (450 total) were examined to calculate the percentage of Ape1-RFP puncta that colocalize with (left) or lie adjacent to (right) Sec13-GFP puncta.

strain because Hrr25 was not sufficiently depleted. Together our findings indicate that Hrr25 is a Ypt1 effector on both the ER–Golgi and macroautophagy pathways. Our findings also suggest that activated Ypt1 can recruit Hrr25 to COPII vesicles that are diverted to the PAS.

The COPII coat plays a role in macroautophagy, but not the Cvt pathway

The TRAPP complexes are upstream activators of Ypt1/Rab1 (Barrowman et al., 2010). We previously showed that Hrr25 phosphorylates two conserved sites in Sec23 that reside in

a domain that also binds to TRAPPI. When these two sites (S742 and T747) are phosphorylated, TRAPPI cannot bind to Sec23 to initiate a new round of vesicle tethering and ER–Golgi traffic is impaired (Lord et al., 2011). We have also shown that TRAPPIII binds to Sec23 (Tan et al., 2013). If TRAPPIII uses the same binding site on Sec23, macroautophagy should be similarly impaired by these phosphomimetic mutations. Quantitative measurements of autophagic activity revealed a decrease in vacuolar alkaline phosphatase activity in the strain that harbored the phosphomimetic mutations, but not the strain that contained the alanine mutations (Fig. 6 C). The *sec23* phosphomimetic mutant was also defective in the delivery of GFP-Atg8 to the vacuole (Fig. 6 D), implying that the Sec23-TRAPP interaction is required for both ER–Golgi traffic and macroautophagy. Thus, macroautophagy appears to be driven by sequential interactions similar to those that drive ER–Golgi traffic.

To ask if phosphorylation of Sec23 at the TRAPP binding site plays a role on the Cvt pathway, we followed the trafficking of aminopeptidase I (Ape1). Trafficking of this vacuolar hydrolase can be assessed by monitoring maturation of the precursor form of Ape1 (prApe1), which is proteolytically activated in the vacuole (mApe1). Consistent with earlier studies showing that the Cvt pathway is independent of the secretory pathway (Klionsky et al., 1992; Ishihara et al., 2001), we did not see a defect in Ape1 processing in the *sec23* phosphomimetic mutant (Fig. 6 E). We did however find that Ape1 fails to be processed in the *hrr25-5* mutant (Fig. 6 F). In agreement with a role for Hrr25 on the Cvt pathway, Hrr25 colocalizes with PAS markers in rich medium, although to a lesser degree than was observed during starvation conditions (Fig. S4 A). Thus, although Sec23 does not appear to play a major role in Ape1 transport, the Cvt and macroautophagy pathways use the same kinase.

We also used a previously published assay (Tan et al., 2013) to ask if COPII vesicles play a role on the Cvt pathway. A significant fraction of COPII vesicles (marked by Sec13-GFP) lie adjacent to the PAS (Tan et al., 2013). When macroautophagy is blocked in *atg* mutants, more COPII vesicles accumulate at the PAS than in WT cells and less vesicles are found adjacent to the PAS (Tan et al., 2013). Sec12, an ER protein responsible for recruiting the COPII coat to ER membranes, behaved differently than Sec13. In WT cells, ∼3% of the Ape1 puncta partially colocalized with Sec12 on the ER, and no increase in colocalization was observed when macroautophagy was blocked in *atg* mutants (Fig. S4 E). COPII vesicle accumulation at the PAS did not increase in *atg1Δ* and *atg13Δ* mutants grown in rich medium (Fig. 6 G), implying that these vesicles are not required on the Cvt pathway and only accumulate as a consequence of blocking macroautophagy during cell stress.

Interestingly, although blocking macroautophagy in several different *atg* mutants (*atg1Δ*, *atg2Δ*, *atg5Δ* and *atg13Δ*) leads to COPII vesicle accumulation at the PAS (Fig. S5, A and B), disrupting this pathway in the *hrr25-5* and *ypt1-3* mutants did not lead to an accumulation when compared with WT (Fig. S5, A and C). Additionally, when *hrr25-5atg1Δ* and *ypt1-3atg1Δ* double mutants were examined, a significant accumulation of COPII vesicles at the PAS was still not observed (Fig. S5, A and C). These epistasis experiments suggest that, in addition to a role in COPII vesicle fusion, Hrr25 may have additional roles in macroautophagy.

Hrr25 and Ypt1 are required for autophagosome biogenesis

The aforementioned findings imply that Hrr25 and Ypt1 may be needed for the biogenesis of the autophagosome. To more directly address this question, we used SIM microscopy to visualize autophagosomes in deconvolved images of WT (Fig. 7 A), *hrr25-5, hrr25Δ*, and *ypt1-3* mutant cells expressing GFP-Atg8 (Fig. 7, A and B). For this analysis, the *hrr25Δ* mutant was also used because it is completely devoid of Hrr25 kinase activity. Whereas Hrr25 is essential for growth in most strain backgrounds, cells deleted for *HRR25* in the W303 strain background grow extremely slowly (Hoekstra et al., 1991). Consistent with a role for Hrr25 and Ypt1 in the biogenesis of autophagosomes, we saw a decrease in autophagosome formation in the *hrr25Δ*, *ypt1-3*, and *hrr25-5* mutants (Fig. 7, A and B), and a defect in the recruitment of GFP-Atg8 to the PAS (Fig. 7 C).

Discussion

Our earlier studies showed that Sec23 is phosphorylated when a COPII vesicle comes in proximity to Hrr25 at the Golgi (Lord et al., 2011). However, it was unclear from these studies how Hrr25 accesses vesicle-bound coat proteins. The realization that COPII vesicles must uncoat on two different pathways prompted us to determine if Hrr25 is directly recruited to the vesicle. The studies we report here imply that activated Ypt1 recruits Hrr25 to vesicles in yeast and mammalian cells. Additionally, although CK1 family members were thought to be constitutively active kinases (Knippschild et al., 2005), we have found that Ypt1 up-regulates Hrr25 kinase activity. Specifically, we showed that Hrr25 kinase activity is almost completely abrogated in the ts *ypt1-3* mutant at 37°C. Consistent with the proposal that Ypt1 directly regulates Hrr25, kinase activity was partially restored when we incubated the inactive kinase with activated Ypt1. These findings imply that Hrr25 functions directly on COPII vesicles and suggest that the steady-state Golgi localization of Hrr25/CK1δ may arise in part from fusion of COPII vesicles with the Golgi (Milne et al., 2001; Lord et al., 2011).

We also found that when macroautophagy is induced, Hrr25 is recruited to the PAS in a Ypt1-dependent manner. The PAS localization of Hrr25 was also dependent on COPII vesicles, as a decrease in the recruitment of Hrr25 to the PAS was observed when vesicle budding was blocked in a *sec12* mutant. Together, these findings imply that when cells are stressed, Ypt1 can recruit Hrr25 to COPII vesicles that are then diverted to the macroautophagy pathway. Consistent with these observations, we found that the *hrr25-5* mutant is defective in macroautophagy.

Although Hrr25 action is a prerequisite for vesicle uncoating, it is not sufficient to uncoat a COPII vesicle (Lord et al., 2011). A possible role for Hrr25 in COPII vesicle fusion may be to stimulate coat release by phosphorylating an uncoating factor. Similarly, on the autophagy pathway, coat release likely precedes vesicle fusion, which may explain why the *hrr25-5* mutant is defective in macroautophagy. Our findings also imply that Hrr25 has additional roles on this pathway. For example, when Hrr25 kinase activity and macroautophagy are impaired, COPII vesicles fail to accumulate at the PAS. Thus, the phosphorylation of one or more PAS components by Hrr25 may be needed for COPII vesicles to accumulate at this site. Alternatively, Hrr25 may play a role in diverting COPII vesicles to the PAS when macroautophagy is induced.

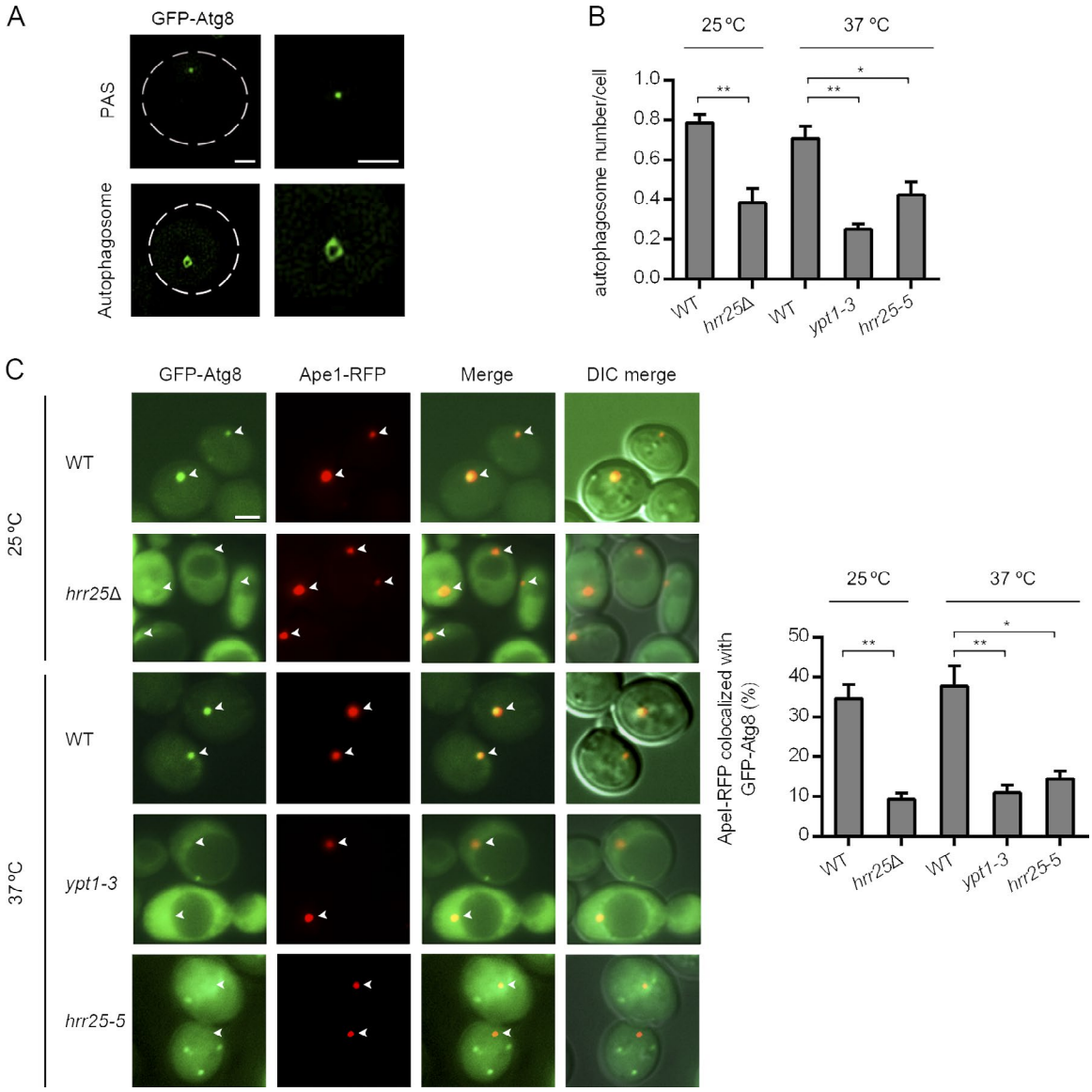

Figure 7. **Hrr25 and Ypt1 are required for autophagosome formation**. (A) WT cells expressing GFP-Atg8 were grown to log phase and treated with 400 ng/ml rapamycin for 1 h at 25°C. Deconvolved images are shown. Bars, 1 µm. (B) WT (SFNY 2663) and *hrr25Δ* (SFNY 2664) cells expressing GFP-Atg8 were treated with 400 ng/ml rapamycin for 30 min at 25°C. The *ypt1-3* (SFNY2662) and *hrr25-5* (SFNY 2622) mutants were treated with rapamycin for 1 h at 37°C. Numbers of autophagosomes were calculated in 300 cells. Error bars represent SEM; $n = 3$; *, $P < 0.05$; **, $P \leq 0.01$; Student's *t* test. (C) WT, *hrr25Δ*, *ypt1-3*, and *hrr25-5* mutant cells expressing GFP-Atg8 and Ape1-RFP (SFNY2668, SFNY2669, SFNY2670, SFNY2671, and SFNY2696) were treated as above. Arrowheads point to the PAS. Bar, 2 µm. Error bars represent SEM; $n = 3$; *, $P < 0.05$; **, $P < 0.01$, Student's *t* test.

Our findings indicate that the COPII subunit Sec23 is not required on the Cvt pathway. Another selective autophagy pathway, antibacterial autophagy, is also independent of COPII vesicles (Huang et al., 2011). Even though COPII vesicles and the COPII coat are not needed on the Cvt pathway, Ypt1 and Hrr25 are essential for Ape1 processing. Two recent reports have shown that phosphorylation of the Ape1 cargo receptor (Atg19) by Hrr25 is required for Ape1 transport to the vacuole (Pfaffenwimmer et al., 2014; Tanaka et al., 2014). As phosphorylation is known to activate this receptor, it will be interesting to see if Ypt1/Rab1 regulates the activation of other cargo receptors via its effector Hrr25/CKIδ. Ypt1/Rab1 may also have other roles in selective autophagy, as its GEF TRAPPIII has recently been shown to be required for the trafficking of Atg9 vesicles on the Cvt pathway (Shirahama-Noda et al., 2013).

In conclusion, the findings we report here explain how a kinase that has multiple locations (Golgi, nucleus, spindle pole bodies, and bud neck; Kafadar et al., 2003; Lusk et al., 2007; Lord et al., 2011) in the cell can be spatially and temporally activated to ensure the fidelity of membrane traffic. Presently, we do not understand how Ypt1 regulates Hrr25 kinase activity. Because the active form of the Rab can restore activity to Hrr25 precipitated from *ypt1-3* mutant cells, Ypt1 could activate Hrr25 via a direct interaction or through another factor that regulates Hrr25. Currently, we are investigating whether Ypt1 also regulates other kinases and if there are other means of activating Hrr25. The findings we describe here are likely to serve

as a paradigm for the role of CK1 family members in membrane traffic, as other coat proteins and vesicle tethering machinery have been reported to interact with Hrr25/CK1δ and its family members (LaGrassa and Ungermann, 2005; Ptacek et al., 2005).

Materials and methods

Media, growth conditions, and yeast strains

Yeast cells were grown at 25°C in yeast extract peptone dextrose media (YPD; 1% yeast extract, 2% peptone, and 2% dextrose) or synthetic minimal media (SMD; 0.67% yeast nitrogen base, 2% dextrose, and auxotrophic amino acids as needed). Nitrogen starvation was induced in synthetic minimal medium lacking nitrogen (SD–N; 0.17% yeast nitrogen base without amino acids and 2% dextrose). For solid media, agar was added to a final concentration of 2%. Key yeast strains used in this study are listed in Table S1.

In vitro phosphorylation of GST-Lst1

GST-Lst1 (5 µg) was purified from *E. coli* onto glutathione Sepharose beads as described previously and incubated with 250 ng of recombinant His_6-Hrr25 (Bhandari et al., 2013) or His_6-Hrr25-5 in 25 µl of kinase buffer (20 mM Tris, pH 7.4, 8 mM EDTA, 10 mM $MgCl_2$). All samples were incubated at 30°C for 1 h before the beads were washed 2 times with PBS and 1 time with 1× CIP buffer (New England BioLabs, Inc.). The beads were resuspended in 1× CIP buffer, and then CIP (1 µl) or buffer (1 µl) was added (60 µl final volume) before each sample was incubated at 37°C for 15 min. At the end of the incubation sample buffer (12.5 µl) was added before heating for 5 min at 95°C.

Analysis of the *hrr25-5* mutant in vitro using the ER–Golgi transport assay

In vitro transport assays were performed as previously described (Groesch et al., 1990; Lian and Ferro-Novick, 1993) using WT and mutant fractions. Briefly, to translocate cargo into ER membranes, permeabilized donor yeast cells were incubated with in vitro translated radiolabeled α-factor for 30 min at 20°C. Subsequently, the donor cells were pelleted, washed, and mixed with an S1 fraction that was prepared as previously described (Groesch et al., 1990). Samples were then incubated in the presence of apyrase or an ATP mix for 90 min at 20°C. At the end of the incubation, the donor cells were pelleted during a 1-min spin at 16,000 *g* and the supernatant and pellet fractions were treated with ConA–Sepharose beads. The beads were washed and equal amounts (20 µl) of each sample were counted using a scintillation counter. To reconstitute transport activity in the *hrr25-5* mutant, recombinant His_6-Hrr25 was preincubated with an S1 fraction for 20 min at 4°C before performing the assay.

The percent of budding was calculated as the counts in supernatant/supernatant+pellet. To determine if α-factor trafficked to the Golgi, another aliquot of the ConA-treated sample (20 µl) was immunoprecipitated with an antibody that recognizes Golgi-specific α1-6 mannose side chains. The percent fusion was calculated as the α1-6 mannose precipitable counts/total ConA counts in the supernatant. The budding and fusion of WT was considered to be maximal.

Analysis of invertase secretion in the *hrr25-5* mutant

WT and mutant cells (6 OD_{600} units) grown overnight at 25°C were resuspended in fresh minimal medium with 2% glucose (supplemented with amino acids), and then preshifted to 37°C for 15 min. At the end of the incubation, the cells were transferred into medium containing 0.1% glucose to derepress the synthesis of invertase and labeled with 250 µCi of [^{35}S] ProMix for 45 min at 37°C. The cells were then washed twice with cold 10 mM sodium azide and resuspended in 160 µl of spheroplasting buffer (1.4 M sorbitol, 50 mM potassium phosphate, pH 7.5, 10 mM sodium azide, 50 mM β-mercaptoethanol, 10 µg of zymolyase/liter OD_{600} unit of cells) for 45 min at 37°C and then centrifuged at 450 *g* for 3 min. An aliquot (120 µl) of supernatant (External) was removed and added to 6 µl of 20% SDS, while the pellet (Internal) were resuspended in 160 µl of 1% SDS. Both samples were immediately heated for 5 min at 100°C. Samples (100 µl) were diluted with PBS + 1% Triton X-100 (900 µl) and centrifuged for 15 min. The supernatant (920 µl) was removed and incubated overnight with 3.5 µl of anti-invertase antibody (a rabbit antiserum prepared against yeast invertase, Ferro-Novick laboratory). Protein A–Sepharose beads (50 µl of a 50% slurry) were then added to the samples for another 90 min before the beads were washed twice with urea wash buffer (2 M urea, 200 mM NaCl, 100 mM Tris, pH 7.6, 1% Triton X-100) and twice with 1% β-mercaptoethanol. The contents of the beads were solubilized in 70 µl of Laemmli sample buffer and analyzed on a 10% SDS polyacrylamide gel.

Immunoprecipitation of Hrr25-HA from yeast lysates

Hrr25-HA was immunoprecipitated from a lysate prepared from 300–500 OD_{600} units of WT and mutant cells grown to log phase and washed with 20 mM Tris, pH 7.5. Cells were converted to spheroplasts in 10 ml of spheroplast buffer (1.4 M sorbitol, 10 mM Na azide, 50 mM KPi, pH 7.5, 0.35% β-mercaptoethanol, 1 mg zymolase) during a 30-min incubation at 37°C. The spheroplasts were collected through a sorbitol cushion (1.7 M sorbitol, 100 mM HEPES, pH 7.4) by centrifugation at 6,400 rpm for 5 min, and the pellet was resuspended in 5 ml of lysis buffer I (20 mM HEPES, pH 7.4, 150 mM NaCl, 1% Triton X-100, 2 mM EDTA, 2 mM PMSF, 2 mM DTT, protease inhibitors). The resuspended pellet was lysed with a dounce homogenizer and insoluble debris was removed by centrifugation at 13,000 rpm for 15 min. Cleared lysate was incubated with 20 µl of anti-HA resin for 2 h at 4°C with rotation. The beads were washed three times with 20 mM HEPES, pH 7.2, and eluted in 50 µl sample buffer by heating for 5 min at 100°C. Samples were then analyzed by Western blot analysis. All Western blots were quantitated using the ChemiDoc MP Imaging System with Image Lab Software.

Cell fractionation

Differential centrifugation was used to separate cells into membrane and soluble fractions as described previously (Lord et al., 2011) with minor modifications. Cells (80 OD_{600} units) were shifted to 37°C for 1 h, centrifuged at 3,000 rpm for 3 min, washed with 10 mM NaN_3/NaF, and converted to spheroplasts in 2 ml of spheroplast buffer (1.4 M sorbitol, 10 mM Na azide, 50 mM KPi, pH 7.5, 0.35% β-mercaptoethanol, 1 mg zymolase). Spheroplasts formed during a 45 min incubation at 37°C were pelleted through a 2 ml sorbitol cushion (1.7 M sorbitol, 100 mM HEPES, pH 7.4) that was spun at 3,000 rpm for 5 min. The pellet was resuspended in 1 ml of lysis buffer (100 mM HEPES, pH 7.2, 1 mM EGTA, 0.2 mM DTT, 1 mM PMSF, and protease inhibitors) using a Dounce homogenizer. The lysate was then spun at 500 g for 2 min and the supernatant (100 µl) was mixed with 50 µl of 3× sample buffer (total fraction, T) and heated to 100°C for 5 min. The remaining portion (500 µl) was centrifuged at 190,000 *g* for 90 min at 4°C. The lipid layer was removed and the supernatant (100 µl) was mixed with 50 µl of 3× sample buffer (supernatant fraction, S) and heated to 100°C for 5 min. The pellet was resuspended in 500 µl of lysis buffer and 100 µl was mixed with 50 µl of 3× sample buffer and heated to 100°C for 5 min (pellet fraction, P).

Purification of recombinant proteins and in vitro binding

GST and human GST-CK1δ were expressed in *E. coli* and immobilized onto glutathione–Sepharose beads (GE Healthcare). Briefly, 500 ml of

cells were grown to early log phase and induced with 0.5 mM IPTG overnight at 18°C. Cells were collected and sonicated in lysis buffer II (1x PBS, 1 mM DTT, and protease inhibitors), and the lysates were centrifuged for 15 min at 26,890 *g*. The cleared lysates were incubated with 1 ml of glutathione-Sepharose beads for 1 h before the beads were washed three times with 25 ml of lysis buffer II and stored at 4°C.

Human His_6-Rab1a Q70L and His_6-Rab1a S25N were purified from *E. coli* using Ni^{2+}-NTA resin (QIAGEN) by the same protocol, except lysis buffer III was used (20 mM HEPES, pH 7.4, 150 mM NaCl, 15 mM Imidazole, and protease inhibitors) and bound His_6-Rab1a was eluted with elution buffer (20 mM HEPES, pH 7.4, 150 mM NaCl, 250 mM Imidazole, and protease inhibitors).

For in vitro binding, His_6-Rab1a S25N and His_6-Rab1a Q70L were incubated with equimolar (0.1 µM) amounts of immobilized GST or GST-CK1δ in binding buffer (50 mM HEPES, pH 7.4, 150 mM NaCl, 2% Triton X-100, 1 mM EDTA, 1 mM DTT, 0.5 mM $MgCl_2$, and protease inhibitors) for 3 h at 4°C with rotation. The beads were washed three times with binding buffer and eluted in 50 µl of sample buffer by heating for 5 min at 100°C. Eluted proteins were examined by SDS-PAGE and Western blot analysis.

Depletion of mammalian Rab1a and Trs85 by shRNA

The shRNA1a that targets human Rab1A, 392–410 (5′-AGAAAG-TAGTAGACTACAC-3′) was constructed in the shRNA expression vector pSilencer 1.0-U6 (Ambion). For transfection, cells (1.8×10^5/well) were seeded in 6-well plates 20 h before transfection and then transfected for 5 h in OPTI-MEM (Invitrogen) with 2 µg DNA (pSilencer 1.0-U6 empty vector control or the shRab1a constructs) in the presence of 5 µl Lipofectamine 2000 Transfection Reagent (Life Technologies). 4 d after transfection, the cells were harvested, lysed, and analyzed by Western blot analysis. For the complementation experiment, a shRab1a-resistant construct was made (5′-AAAAAG-GTCGTAGACTACACA-3′) in the target sequence of shRab1a. 2 d after shRNA transfection, the cells were transfected with the shRNA-resistant construct. After 48 h, the cells were harvested and analyzed by Western blot analysis.

For depletion of Trs85 by shRNA, two shTrs85 sequences were constructed in the shRNA expression vector pSilencer 1.0-U6. shTrs85-1 targets human Trs85, 1568–1586 (5′-CAGCTCTCCTA-ATACGGTT-3′), whereas shTrs85-2 targets human Trs85, 1636–1654 (5′-GCACATTGCTTTATAAACA-3′). HeLa cells were transfected with mock or the shTrs85 constructs as above. 4 d after transfection, the cells were harvested, lysed, and analyzed by Western blot analysis. For the complementation experiments, two shRNA-resistant constructs were made, called shTrs85-1 rescue and shTrs85-2 rescue. shTrs85-1 rescue expressed myc-Trs85 that contained three silent mutations (A1578T, G1584C, and T1585C) in the target sequence of shTrs85-1. shTrs85-2 rescue expressed myc-Trs85 that contained three silent mutations (T1641C, T1647C, and A1650C) in the target sequence of shTrs85-2. 2 d after shRNA transfection, the cells were transfected with the shRNA-resistant construct. After 48 h, the cells were harvested and analyzed by Western blot analysis.

Kinase assay

Cells expressing Hrr25-HA were grown overnight in SC-URA medium to early log phase and shifted to 37°C for 2 h. The cells were lysed and Hrr25-HA was immunoprecipitated with anti-HA resin as described above, or, 2 mg of lysate was incubated with 1 µg of anti-HA antibody (monoclonal antibody purchased from Roche, clone 12CA5) for 2 h at 4°C followed by the addition of 20 µl of Protein A–Sepharose beads. The beads were preincubated with 10 mg/ml of BSA for 1 h before the addition of lysate. After 1 h, the beads were washed three times with lysis buffer (50 mM Tris-HCl, pH 7.4, 100 mM NaCl, 5 mM EDTA, 1 mM PMSF, 1% Triton X-100, and 1× protease inhibitor mixture [Roche]), and two times with kinase buffer (50 mM HEPES, pH 7.4, 5 mM $MgCl_2$, 0.2% NP-40, and 1 mM DTT). The kinase activity of immunopurified Hrr25-HA was assayed in a 50-µl reaction volume using 1 µg of myelin basic protein (MBP) as substrate, as previously described (Wang et al., 2013). For the reconstitution assay, the precipitated beads were preincubated with purified bacterially expressed recombinant Ypt1-His_6 (Q67L) protein in 10 µl of kinase buffer for 15 min at 25°C before the addition of MBP and 1 µCi ^{32}P γATP. The final reaction (50 µl) was terminated by the addition of 20 µl of 5× SDS sample buffer and incubated at 95°C for 5 min.

Immunoprecipitation and CIP treatment of Lst1

A total of 100 OD_{600} units of exponentially grown cells were shifted to 37°C for 1 h, collected by centrifugation, and washed with 5 ml of 20 mM NaF. Cells were resuspended in 2 ml of spheroplast buffer (as in Cell fractionation, except with 0.25 mg zymolase), incubated for 30 min at 37°C, and collected through a 4-ml sorbitol cushion. The pellet was resuspended in 1 ml of IP buffer (50 mM Tris, pH 8.0, 100 mM NaCl, 10 mM $MgCl_2$, 0.5% Triton X-100, 1 mM DTT, 1 mM PMSF, phosphatase, and protease inhibitors) and lysed with a dounce homogenizer, and insoluble material was removed by centrifugation at 13,000 rpm for 15 min. The cleared lysate (4 mg) was incubated with anti-Lst1 antibody (rabbit antiserum prepared against GST-Lst1, Ferro-Novick laboratory) for 1 h at 4°C, and immune complexes were collected by incubation with 40 µl of Protein A beads for 1 h at 4°C before the samples were washed three times with IP buffer. For the CIP assays, the Protein A beads were washed three times with CIP buffer (New England BioLabs, Inc.) supplemented with protease inhibitor cocktail (Roche). The beads were resuspended in 100 µl of CIP buffer with CIP (0.5 U/µl) or with CIP plus 50 mM EDTA and incubated at 37°C for 20 min. At the end of the incubation, the samples were mixed with 3× sample buffer and heated at 100°C for 5 min.

Microscopy

Cells were grown overnight at 25°C in YPD medium to an OD_{600} between 0.5–1.0. To induce macroautophagy, cells were washed and shifted to SD–N medium for 1–4 h or treated with 400 ng/ml rapamycin for 30–60 min. Cells were visualized at 25°C with a an Axio Imager Z1 fluorescence microscope (Carl Zeiss) using a 100× 1.3 NA oil-immersion objective. Images were captured with a AxioCam MRm digital camera and analyzed using AxioVision software (Carl Zeiss). To analyze autophagosome and phagophore formation, cells were fixed with 3.7% formaldehyde at 25°C for 30 min and visualized at 25°C on an Applied Precision DeltaVision OMX Super Resolution System using an Olympus UPlanSApo 100× 1.4 NA oil objective. Images were taken with a Photometrics Evolve 512 EMCCD camera. The data were acquired and processed using Delta Vision OMX Master Control software and SoftWoRx reconstruction and analysis software.

Pho8Δ60 assay

Alkaline phosphatase assays were performed as described previously (Klionsky, 2007). Briefly, cells were grown overnight at 25°C to log phase, washed twice and then incubated in SD–N medium for 2 h at 37°C to induce macroautophagy. The cells were then lysed in lysis buffer IV (20 mM PIPES, pH 7.2, 0.5% Triton X-100, 50 mM KCl, 100 mM potassium acetate, 10 mM $MgSO_4$, 10 µM $ZnSO_4$, and 1 mM PMSF) using glass beads. Lysates were assayed at 37°C in reaction buffer (1.25 mM p-nitrophenyl phosphate, 250 mM Tris-HCl, pH 8.5, 0.4% Triton X-100, 10 mM $MgSO_4$, and 10 µM $ZnSO_4$) and the reaction was stopped with 500 µl of stop buffer (1 M glycine/KOH, pH

11.0). The OD_{400} value was determined and normalized to protein concentration using the Bradford method.

Ape1 processing assay

Cells were grown overnight at 25°C to early log phase, shifted to 37°C for 2 h, and pelleted (2.5 OD_{600} units). The resuspended cell pellet (100 µl H_2O and 100 µl 0.2 M NaOH) was incubated for 5 min at room temperature, centrifuged, resuspended in 50 µl of sample buffer, and heated for 5 min at 100°C. Samples were subsequently analyzed using Western blot analysis with anti-Ape1 antibody (rabbit antiserum prepared against His_6-Ape1 at the Ferro-Novick laboratory).

Online supplemental material

Fig. S1 shows that Hrr25-5 is defective in kinase activity. Fig. S2 shows that Rab1 regulates the recruitment of CK1δ to membranes. Fig. S3 shows that Ypt1 regulates the phosphorylation of the COPII coat. Fig. S4 shows that Hrr25 is recruited to the PAS. Fig. S5 shows Hrr25 and Ypt1 are required for the accumulation of COPII vesicles at the PAS in *atgΔ* mutants. Online supplemental material is available at http://www.jcb.org/cgi/content/full/jcb.201408075/DC1.

Acknowledgments

We thank Wenyun Zhou and Shuliang Chen for technical assistance and Chris Lord for help with the in vitro transport assay. We also thank the University of California, San Diego School of Medicine Microscopy Core for use of the Applied Precision Delta Vision OMX Super Resolution System.

Salary support for J. Wang, S. Menon, J. Zhang, J. Ding, S. Cervantes, and S. Ferro-Novick was provided by the Howard Hughes Medical Institute. E. Miller was supported by NIGMS (R01GM085089), and Y. Jiang was supported by NCI (R21CA169186).

The authors declare no competing financial interests.

Submitted: 18 August 2014
Accepted: 10 June 2015

References

Bacon, R.A., A. Salminen, H. Ruohola, P. Novick, and S. Ferro-Novick. 1989. The GTP-binding protein Ypt1 is required for transport in vitro: the Golgi apparatus is defective in ypt1 mutants. *J. Cell Biol.* 109:1015–1022. http://dx.doi.org/10.1083/jcb.109.3.1015

Ballew, N., Y. Liu, and C. Barlowe. 2005. A Rab requirement is not bypassed in SLY1-20 suppression. *Mol. Biol. Cell.* 16:1839–1849. http://dx.doi.org/10.1091/mbc.E04-08-0725

Barrowman, J., D. Bhandari, K. Reinisch, and S. Ferro-Novick. 2010. TRAPP complexes in membrane traffic: convergence through a common Rab. *Nat. Rev. Mol. Cell Biol.* 11:759–763. http://dx.doi.org/10.1038/nrm2999

Bhandari, D., J. Zhang, S. Menon, C. Lord, S. Chen, J.R. Helm, K. Thorsen, K.D. Corbett, J.C. Hay, and S. Ferro-Novick. 2013. Sit4p/PP6 regulates ER-to-Golgi traffic by controlling the dephosphorylation of COPII coat subunits. *Mol. Biol. Cell.* 24:2727–2738. http://dx.doi.org/10.1091/mbc.E13-02-0114

Ge, L., D. Melville, M. Zhang, and R. Schekman. 2013. The ER-Golgi intermediate compartment is a key membrane source for the LC3 lipidation step of autophagosome biogenesis. *eLife.* 2:e00947. http://dx.doi.org/10.7554/eLife.00947

Ge, L., M. Zhang, and R. Schekman. 2014. Phosphatidylinositol 3-kinase and COPII generate LC3 lipidation vesicles from the ER-Golgi intermediate compartment. *eLife.* 3:e04135. http://dx.doi.org/10.7554/eLife.04135

Graef, M., J.R. Friedman, C. Graham, M. Babu, and J. Nunnari. 2013. ER exit sites are physical and functional core autophagosome biogenesis components. *Mol. Biol. Cell.* 24:2918–2931. http://dx.doi.org/10.1091/mbc.E13-07-0381

Groesch, M.E., H. Ruohola, R. Bacon, G. Rossi, and S. Ferro-Novick. 1990. Isolation of a functional vesicular intermediate that mediates ER to Golgi transport in yeast. *J. Cell Biol.* 111:45–53. http://dx.doi.org/10.1083/jcb.111.1.45

Hoekstra, M.F., R.M. Liskay, A.C. Ou, A.J. DeMaggio, D.G. Burbee, and F. Heffron. 1991. HRR25, a putative protein kinase from budding yeast: association with repair of damaged DNA. *Science.* 253:1031–1034. http://dx.doi.org/10.1126/science.1887218

Huang, J., C.L. Birmingham, S. Shahnazari, J. Shiu, Y.T. Zheng, A.C. Smith, K.G. Campellone, W.D. Heo, S. Gruenheid, T. Meyer, et al. 2011. Antibacterial autophagy occurs at PI(3)P-enriched domains of the endoplasmic reticulum and requires Rab1 GTPase. *Autophagy.* 7:17–26. http://dx.doi.org/10.4161/auto.7.1.13840

Ishida, M., N. Ohbayashi, Y. Maruta, Y. Ebata, and M. Fukuda. 2012. Functional involvement of Rab1A in microtubule-dependent anterograde melanosome transport in melanocytes. *J. Cell Sci.* 125:5177–5187. http://dx.doi.org/10.1242/jcs.109314

Ishihara, N., M. Hamasaki, S. Yokota, K. Suzuki, Y. Kamada, A. Kihara, T. Yoshimori, T. Noda, and Y. Ohsumi. 2001. Autophagosome requires specific early Sec proteins for its formation and NSF/SNARE for vacuolar fusion. *Mol. Biol. Cell.* 12:3690–3702. http://dx.doi.org/10.1091/mbc.12.11.3690

Kafadar, K.A., H. Zhu, M. Snyder, and M.S. Cyert. 2003. Negative regulation of calcineurin signaling by Hrr25p, a yeast homolog of casein kinase I. *Genes Dev.* 17:2698–2708. http://dx.doi.org/10.1101/gad.1140603

Kirisako, T., M. Baba, N. Ishihara, K. Miyazawa, M. Ohsumi, T. Yoshimori, T. Noda, and Y. Ohsumi. 1999. Formation process of autophagosome is traced with Apg8/Aut7p in yeast. *J. Cell Biol.* 147:435–446. http://dx.doi.org/10.1083/jcb.147.2.435

Klionsky, D.J. 2007. Monitoring autophagy in yeast: the Pho8Delta60 assay. *Methods Mol. Biol.* 390:363–371. http://dx.doi.org/10.1007/978-1-59745-466-7_24

Klionsky, D.J., R. Cueva, and D.S. Yaver. 1992. Aminopeptidase I of Saccharomyces cerevisiae is localized to the vacuole independent of the secretory pathway. *J. Cell Biol.* 119:287–299. http://dx.doi.org/10.1083/jcb.119.2.287

Knippschild, U., A. Gocht, S. Wolff, N. Huber, J. Löhler, and M. Stöter. 2005. The casein kinase 1 family: participation in multiple cellular processes in eukaryotes. *Cell. Signal.* 17:675–689. http://dx.doi.org/10.1016/j.cellsig.2004.12.011

LaGrassa, T.J., and C. Ungermann. 2005. The vacuolar kinase Yck3 maintains organelle fragmentation by regulating the HOPS tethering complex. *J. Cell Biol.* 168:401–414. http://dx.doi.org/10.1083/jcb.200407141

Lian, J.P., and S. Ferro-Novick. 1993. Bos1p, an integral membrane protein of the endoplasmic reticulum to Golgi transport vesicles, is required for their fusion competence. *Cell.* 73:735–745. http://dx.doi.org/10.1016/0092-8674(93)90253-M

Lord, C., D. Bhandari, S. Menon, M. Ghassemian, D. Nycz, J. Hay, P. Ghosh, and S. Ferro-Novick. 2011. Sequential interactions with Sec23 control the direction of vesicle traffic. *Nature.* 473:181–186. http://dx.doi.org/10.1038/nature09969

Lusk, C.P., D.D. Waller, T. Makhnevych, A. Dienemann, M. Whiteway, D.Y. Thomas, and R.W. Wozniak. 2007. Nup53p is a target of two mitotic kinases, Cdk1p and Hrr25p. *Traffic.* 8:647–660. http://dx.doi.org/10.1111/j.1600-0854.2007.00559.x

Lynch-Day, M.A., D. Bhandari, S. Menon, J. Huang, H. Cai, C.R. Bartholomew, J.H. Brumell, S. Ferro-Novick, and D.J. Klionsky. 2010. Trs85 directs a Ypt1 GEF, TRAPPIII, to the phagophore to promote autophagy. *Proc. Natl. Acad. Sci. USA.* 107:7811–7816. http://dx.doi.org/10.1073/pnas.1000063107

Mashhoon, N., A.J. DeMaggio, V. Tereshko, S.C. Bergmeier, M. Egli, M.F. Hoekstra, and J. Kuret. 2000. Crystal structure of a conformation-selective casein kinase-1 inhibitor. *J. Biol. Chem.* 275:20052–20060. http://dx.doi.org/10.1074/jbc.M001713200

Milne, D.M., P. Looby, and D.W. Meek. 2001. Catalytic activity of protein kinase CK1 delta (casein kinase 1delta) is essential for its normal subcellular localization. *Exp. Cell Res.* 263:43–54. http://dx.doi.org/10.1006/excr.2000.5100

Murakami, A., K. Kimura, and A. Nakano. 1999. The inactive form of a yeast casein kinase I suppresses the secretory defect of the sec12 mutant. Implication of negative regulation by the Hrr25 kinase in the vesicle budding from the endoplasmic reticulum. *J. Biol. Chem.* 274:3804–3810. http://dx.doi.org/10.1074/jbc.274.6.3804

Nakatogawa, H., K. Suzuki, Y. Kamada, and Y. Ohsumi. 2009. Dynamics and diversity in autophagy mechanisms: lessons from yeast. *Nat. Rev. Mol. Cell Biol.* 10:458–467. http://dx.doi.org/10.1038/nrm2708

Novick, P., and R. Schekman. 1979. Secretion and cell-surface growth are blocked in a temperature-sensitive mutant of Saccharomyces cerevisiae.

Proc. Natl. Acad. Sci. USA. 76:1858–1862. http://dx.doi.org/10.1073/pnas.76.4.1858

Pfaffenwimmer, T., W. Reiter, T. Brach, V. Nogellova, D. Papinski, M. Schuschnig, C. Abert, G. Ammerer, S. Martens, and C. Kraft. 2014. Hrr25 kinase promotes selective autophagy by phosphorylating the cargo receptor Atg19. *EMBO Rep.* 15:862–870. http://dx.doi.org/10.15252/embr.201438932

Ptacek, J., G. Devgan, G. Michaud, H. Zhu, X. Zhu, J. Fasolo, H. Guo, G. Jona, A. Breitkreutz, R. Sopko, et al. 2005. Global analysis of protein phosphorylation in yeast. *Nature.* 438:679–684. http://dx.doi.org/10.1038/nature04187

Rossi, G., J.A. Yu, A.P. Newman, and S. Ferro-Novick. 1991. Dependence of Ypt1 and Sec4 membrane attachment on Bet2. *Nature.* 351:158–161. http://dx.doi.org/10.1038/351158a0

Shimoni, Y., T. Kurihara, M. Ravazzola, M. Amherdt, L. Orci, and R. Schekman. 2000. Lst1p and Sec24p cooperate in sorting of the plasma membrane ATPase into COPII vesicles in Saccharomyces cerevisiae. *J. Cell Biol.* 151:973–984. http://dx.doi.org/10.1083/jcb.151.5.973

Shirahama-Noda, K., S. Kira, T. Yoshimori, and T. Noda. 2013. TRAPPIII is responsible for vesicular transport from early endosomes to Golgi, facilitating Atg9 cycling in autophagy. *J. Cell Sci.* 126:4963–4973. http://dx.doi.org/10.1242/jcs.131318

Suzuki, K., T. Kirisako, Y. Kamada, N. Mizushima, T. Noda, and Y. Ohsumi. 2001. The pre-autophagosomal structure organized by concerted functions of APG genes is essential for autophagosome formation. *EMBO J.* 20:5971–5981. http://dx.doi.org/10.1093/emboj/20.21.5971

Suzuki, K., M. Akioka, C. Kondo-Kakuta, H. Yamamoto, and Y. Ohsumi. 2013. Fine mapping of autophagy-related proteins during autophagosome formation in Saccharomyces cerevisiae. *J. Cell Sci.* 126:2534–2544. http://dx.doi.org/10.1242/jcs.122960

Tan, D., Y. Cai, J. Wang, J. Zhang, S. Menon, H.T. Chou, S. Ferro-Novick, K.M. Reinisch, and T. Walz. 2013. The EM structure of the TRAPPIII complex leads to the identification of a requirement for COPII vesicles on the macroautophagy pathway. *Proc. Natl. Acad. Sci. USA.* 110:19432–19437. http://dx.doi.org/10.1073/pnas.1316356110

Tanaka, C., L.J. Tan, K. Mochida, H. Kirisako, M. Koizumi, E. Asai, M. Sakoh-Nakatogawa, Y. Ohsumi, and H. Nakatogawa. 2014. Hrr25 triggers selective autophagy-related pathways by phosphorylating receptor proteins. *J. Cell Biol.* 207:91–105. http://dx.doi.org/10.1083/jcb.201402128

Trimble, R.B., and F. Maley. 1977. Subunit structure of external invertase from Saccharomyces cerevisiae. *J. Biol. Chem.* 252:4409–4412.

Wang, J., S. Menon, A. Yamasaki, H.T. Chou, T. Walz, Y. Jiang, and S. Ferro-Novick. 2013. Ypt1 recruits the Atg1 kinase to the preautophagosomal structure. *Proc. Natl. Acad. Sci. USA.* 110:9800–9805. http://dx.doi.org/10.1073/pnas.1302337110

Winslow, A.R., C.W. Chen, S. Corrochano, A. Acevedo-Arozena, D.E. Gordon, A.A. Peden, M. Lichtenberg, F.M. Menzies, B. Ravikumar, S. Imarisio, et al. 2010. α-Synuclein impairs macroautophagy: implications for Parkinson's disease. *J. Cell Biol.* 190:1023–1037. http://dx.doi.org/10.1083/jcb.201003122

Zanetti, G., K.B. Pahuja, S. Studer, S. Shim, and R. Schekman. 2012. COPII and the regulation of protein sorting in mammals. *Nat. Cell Biol.* 14:20–28. http://dx.doi.org/10.1038/ncb2390